

The Response of the Nordic Seas to Wintertime Sea Ice Retreat

YUE WU,^a DAVID P. STEVENS,^a IAN A. RENFREW,^b AND XIAOMING ZHAI^b

^a*School of Mathematics, Centre for Ocean and Atmospheric Sciences, University of East Anglia, Norwich, United Kingdom*

^b*School of Environmental Sciences Centre for Ocean and Atmospheric Sciences, University of East Anglia, Norwich, United Kingdom*

(Manuscript received 4 December 2020, in final form 19 March 2021)

ABSTRACT: The ocean response to wintertime sea ice retreat is investigated in the coupled climate model HiGEM. We focus on the marginal ice zone and adjacent waters of the Nordic seas, where the air–sea temperature difference can be large during periods of off-ice winds promoting high heat flux events. Both control and transient climate model ensembles are examined, which allows us to isolate the ocean response due to sea ice retreat from the response due to climate change. As the wintertime sea ice edge retreats toward the Greenland coastline, it exposes waters that were previously covered by ice, which enhances turbulent heat loss and mechanical mixing, leading to a greater loss of buoyancy and deeper vertical mixing in this location. However, under global warming, the buoyancy loss is inhibited as the atmosphere warms more rapidly than the ocean, which reduces the air–sea temperature difference. This occurs most prominently farther away from the retreating ice edge, over the Greenland Sea Gyre. Over the gyre the upper ocean also warms significantly, resulting in a more stratified water column and, as a consequence, a reduction in the depth of convective mixing. In contrast, closer to the coast the effect of global warming is overshadowed by the effect of the sea ice retreat, leading to significant changes in ocean temperature and salinity in the vicinity of the marginal ice zone.

KEYWORDS: Sea ice; Atmosphere–ocean interaction; Ocean circulation


1. Introduction


The Nordic seas, connecting the Arctic Ocean and the North Atlantic Ocean, play an essential role in providing the dense waters of the North Atlantic. Atmosphere–ocean coupling is most intense in the extended winter when deep convection takes place in the Nordic seas (Rudels et al. 2005; Budéus et al. 2004; Brakstad et al. 2019). This is when the greatest air–sea heat and moisture transfers take place, impacting subpolar water mass transformations and ocean circulation (Marshall and Schott 1999; Blindheim and Østerhus 2005). Convective mixing connects the near surface with the deep ocean (Marshall and Schott 1999), while sea ice cover acts as a barrier to heat fluxes between the atmosphere and ocean (Day et al. 2013).

Convection can take place in each of the basins of the Nordic seas, with the deepest convection in the Greenland Sea, often reaching depths greater than 800 m (Swift and Aagaard 1981). Open ocean convection traditionally requires a preconditioned state where a cyclonic gyre circulation results in domed isopycnals and reduced stratification, which enables persistent buoyancy loss from cooling by the atmosphere or sea ice formation to trigger convective mixing (Marshall and Schott 1999). The majority of high heat flux events (60%–80%) in the

Nordic seas are triggered by marine cold-air outbreaks, with the most intense occurring along the ice edge from the Fram Strait to the east of Greenland Sea (Papritz and Spengler 2017). Sea ice cover affects heat fluxes by modulating the area of exposed ocean in contact with the atmosphere. For example, Pope et al. (2020) found changes in surface heat fluxes of the Iceland and Greenland Sea Gyres of up to 15%, for different sea ice distributions. Sea ice extent in this region is influenced by synoptic-scale weather regimes, such as the North Atlantic Oscillation, and so there is interannual variability associated with in these regimes (Pope et al. 2020). A reduction in surface heat loss is likely to limit the depth of convection, which potentially decreases the supply of the densest overflow waters to the North Atlantic (Moore et al. 2015).

Another important factor at the ocean surface is wind forcing from the atmosphere. Deeper convection could be a consequence of increased cyclonic wind forcing that enhances the cyclonic gyre circulation (Malmberg and Jónsson 1997). As elaborated by Jónsson (1992), over the Iceland Sea positive wind stress curl gives rise to a cyclonic circulation and Ekman upwelling in the gyre, leading to a densification and lower stability of the water column in the gyre, where deep convection is more likely to take place. Meincke et al. (1992) also found that the wind stress curl is correlated with wintertime convection in the Greenland Sea on decadal and interannual time scales. The atmospheric forcing also modifies Atlantic Water inflow and recirculating Atlantic Water through the East Greenland Current (Chatterjee et al. 2018).

 Denotes content that is immediately available upon publication as open access.

 Supplemental information related to this paper is available at the Journals Online website: <https://doi.org/10.1175/JCLI-D-20-0932.s1>.

Corresponding author: Yue Wu, yue.wu@uea.ac.uk

DOI: 10.1175/JCLI-D-20-0932.1



This article is licensed under a Creative Commons Attribution 4.0 license (<http://creativecommons.org/licenses/by/4.0/>).

Reduced sea ice extent was recorded during the warm period from the 1920s to the 1940s, followed by sea ice expansion during a cool period from the 1960s to the 1970s (Bengtsson et al. 2004; Shindell and Faluvegi 2009). The cool period in the early 1970s is associated with strong deep convection from the surface to near the sea floor (~3500 m) in the central Greenland Sea (Malmberg 1983), where the formation of very dense Greenland Sea Deep Water (GSDW) takes place. When this is occurring, the Greenland Sea is one of the main sources of the dense water that overflows to the North Atlantic (Carmack and Aagaard 1973; Malmberg 1983; Aagaard et al. 1985). However, convection in the central Greenland Sea has weakened to intermediate depths (~1000 m) since the mid-1980s (Ronski and Budéus 2005), resulting in the occupation of locally formed Arctic Intermediate Water and the absence of ventilated GSDW (Rhein 1991; Schlosser et al. 1991; Meincke et al. 1997). This can be associated with atmospheric heat fluxes decreasing by 20% over the Greenland Sea during this period (Moore et al. 2015).

As global warming is amplified in the Arctic, wintertime sea ice decline has accelerated since the 1990s (Vaughan et al. 2013). The dramatic loss of sea ice in recent decades is creating a new atmosphere–ice–ocean environment where large swathes of the ocean that were previously ice-covered are now exposed to the atmosphere. Despite the largest sea ice loss occurring in summer and autumn (Vaughan et al. 2013), the sea ice loss in winter and spring may be just as important for the climate system. Brakstad et al. (2019) observed that sea ice formation had a slight contribution to a deeper mixing in the Greenland Sea Gyre during the late 1980s and early 1990s, but the contribution did not exceed 400 m. While Våge et al. (2018) found a reduced sea ice cover has enhanced mixing in the region of sea ice retreat in some recent years, resulting in a re-ventilation of the Atlantic-origin water that is transported toward Denmark Strait.

While some studies have investigated ocean convection and circulation changes in the Nordic seas under reduced sea ice conditions (Moore et al. 2015; Våge et al. 2018; Brakstad et al. 2019; Pope et al. 2020), there is little work focusing on the impact of anthropogenic climate change, and none that uses coupled climate models. To what extent changes are part of natural variability or a result of a warming climate is still an open question. Here we examine how sea ice retreat, with and without global warming, impacts water mass transformation in the Nordic seas. We focus on the marginal ice zone and adjacent waters, where the air–sea temperature difference can be large, and the Greenland Sea Gyre, where the deepest convection can occur. To separate the impact of sea ice retreat due to anthropogenic forcing from that associated with natural variability, we compare model output from experiments with and without anthropogenic forcing. This allows us to isolate the impacts on the ocean of sea ice retreat versus sea ice retreat plus global warming. Section 2 describes the model, numerical experiments, and analysis methods. The results are presented in sections 3 to 5, including the evolution of sea ice, surface variables, heat fluxes, and ocean thermodynamical structure for the two scenarios. In section 6, we discuss convective mixing at the sea ice edge and the effects of global warming. Concluding remarks are given in section 7.

2. Methods

a. Model and experiments

Our study is based on model experiments using the High-Resolution Global Environmental Model (HiGEM), which is a fully coupled atmosphere–ice–ocean climate model. It is based on the Met Office Hadley Centre Global Environmental Model version 1 (HadGEM1) with higher resolution in both the atmosphere and ocean. A comprehensive description was given in Shaffrey et al. (2009). The model has a horizontal resolution of $5/6^\circ$ latitude \times $5/4^\circ$ longitude in the atmosphere, and $1/3^\circ \times 1/3^\circ$ in the ocean and sea ice. There are 38 vertical levels in the atmosphere and 40 vertical levels in the ocean. The sea ice component is based on the Community Ice Code (CICE; Hunke and Dukowicz 1997) elastic–viscous–plastic (EVP) model (Lipscomb and Hunke 2004). Shaffrey et al. (2009) provided an overview of the model's performance. They show that in the Nordic seas, the climatology of the model is an improvement over its lower-resolution counterpart and is consistent with observations in terms of ocean volume transport (Hansen and Østerhus 2000; Fahrbach et al. 2001; Jónsson and Briem 2003; Macrander et al. 2005), precipitation (Xie and Arkin 1997), winter sea ice, sea level pressure (Uppala et al. 2005), and sea surface temperature and salinity (Conkright et al. 2002). Several other studies have also demonstrated that HiGEM has a good representation of the Arctic when compared with observations (Lique et al. 2015; de Boer et al. 2018).

We use two ensembles of experiments. First, an ensemble of three control runs (CTRL) from nominal year 1957 to 2019. Here the initial conditions are from three different consecutive days at the end of a 65-yr control run forced with constant external forcing for the late 1950s [further details in Shaffrey et al. (2017)]. The long-term drifts in ocean temperatures below 500 m were reported as small. In CTRL the greenhouse gas concentrations are kept constant at 1957 levels. Second, we use an ensemble of four climate change runs (referred to as GW, for global warming). These are initialized in the same manner as the CTRL ensemble and are also run from 1957 to 2019 with greenhouse gas emissions following the CMIP5 RCP Historical scenario from 1957 to 2005 and CMIP5 RCP4.5 scenario afterward [further details in Shaffrey et al. (2017) and Robson et al. (2018)].

The two ensembles, CTRL and GW, allow us to examine the response of the ocean to sea ice retreat and attribute elements of the response to natural variability or anthropogenic forcing. The GW ensemble includes natural variability and changes from anthropogenic forcing that alters ocean convection in the neighborhood of the region of sea ice retreat, while the CTRL ensemble allows us to identify differences in convective processes due only to natural variability.

b. Analysis methods

In the Arctic, sea ice reaches its maximum extent in March (Cavalieri and Parkinson 2012), so here monthly means for March are used as representative of winter. Two regions are selected for analysis: box A is sited where there is a large interannual sea ice variance; box B is located immediately to the

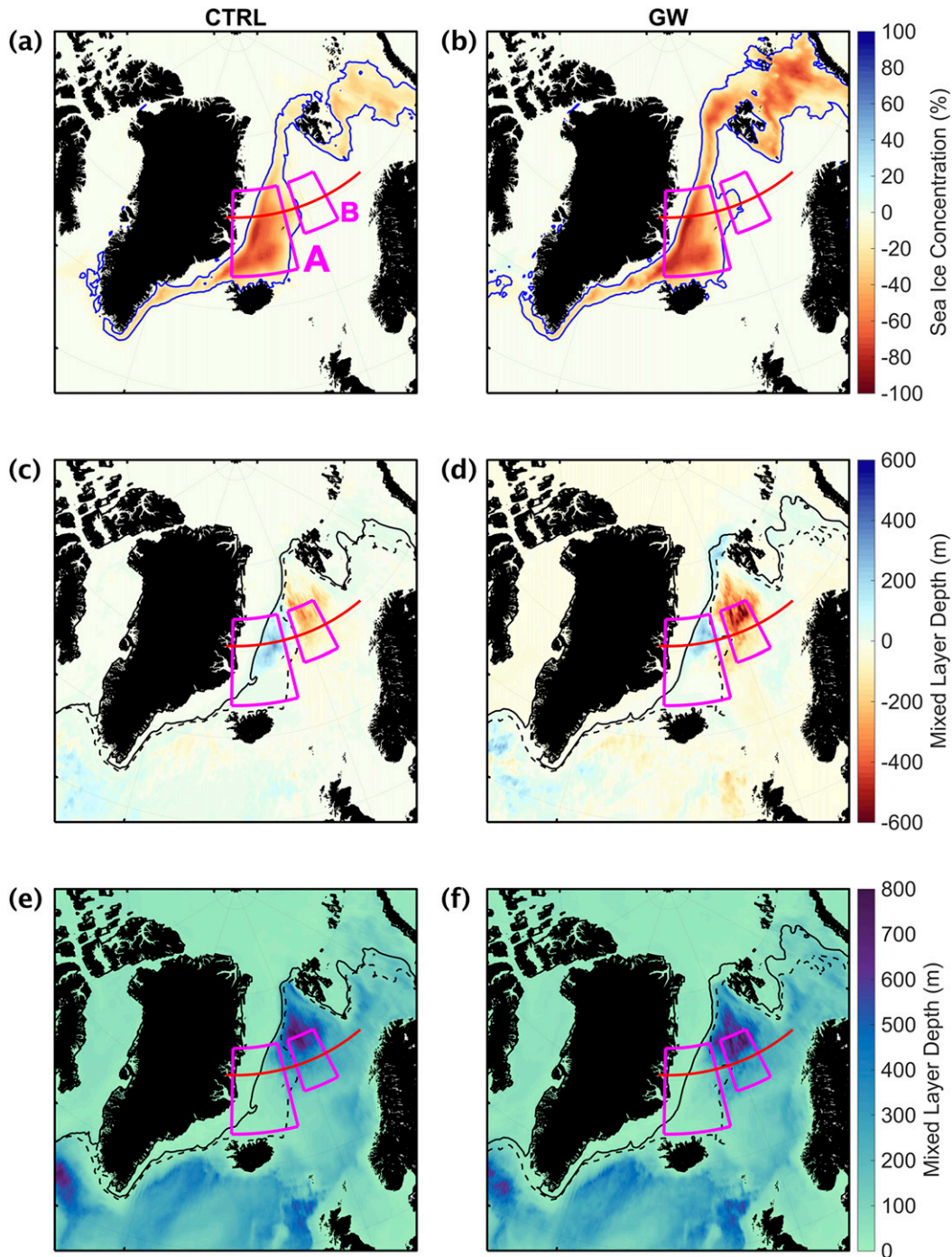


FIG. 1. Differences of (a),(b) sea ice concentration (SIC) and (c),(d) mixed layer depth (MLD) between low and high sea ice conditions (low minus high), plus (e),(f) spatial distributions of MLD for high sea ice conditions, in the (left) CTRL and (right) GW scenarios. In (a) and (b) the blue solid contours depict a SIC change of 0.1. In (c)–(f) the solid and dashed contours mark a SIC of 0.15 in low and high years, respectively. Overlaid on all panels are the areas of focus for the analysis: box A, box B, and the 72.5°N line of latitude.

east and encompasses part of the Greenland Sea Gyre, where the deepest convection takes place (Fig. 1).

Composites are constructed for high and low sea ice years for both CTRL and GW. For CTRL, high/low sea ice years are identified

individually as years when the sea ice extent in box A is outside one standard deviation of the mean. There are 30 (32) individual years for the high (low) sea ice composites, out of 189 experimental years over the three ensemble members. We label these composites

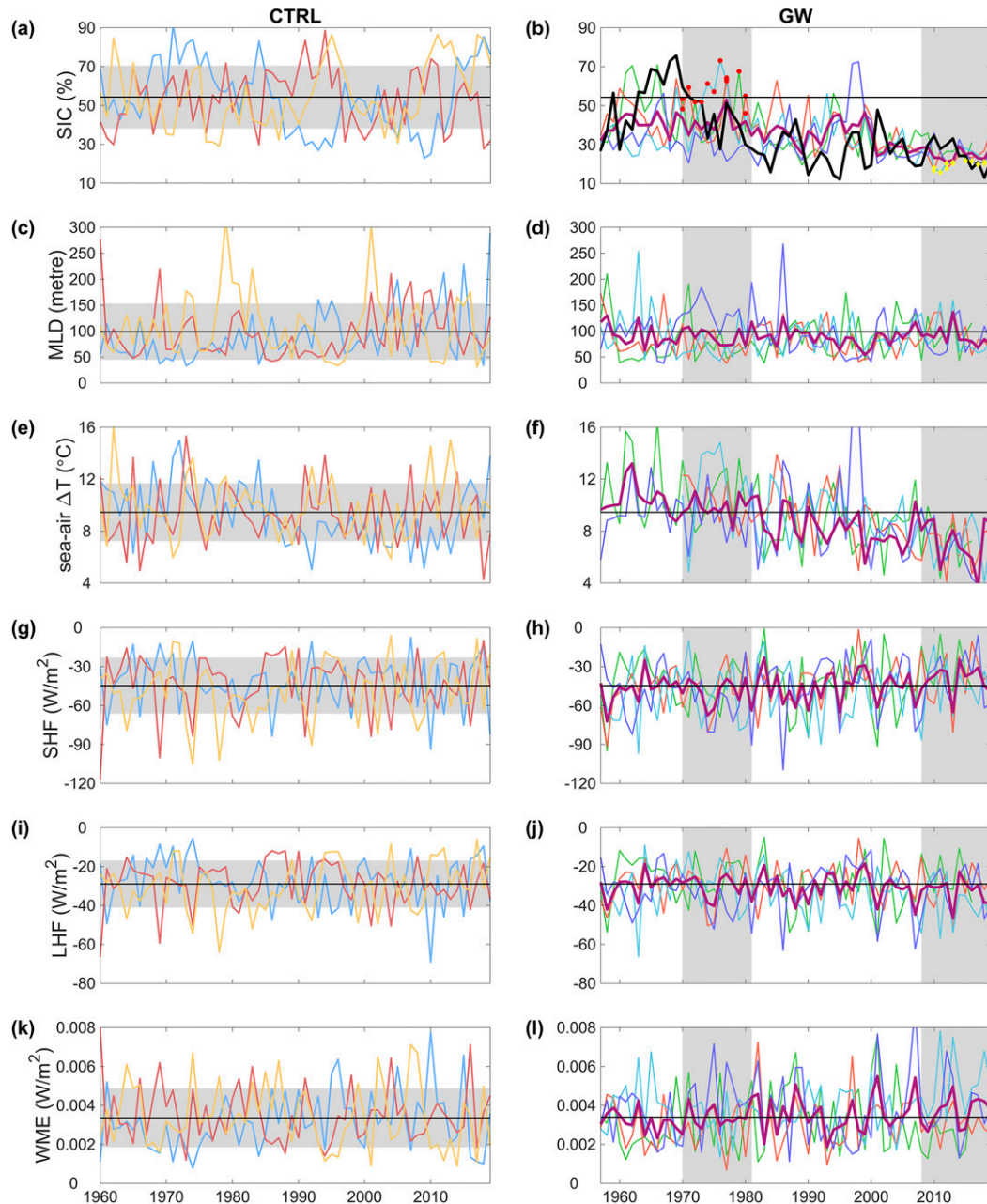


FIG. 2. Time evolution of box A area-averaged variables from the (left) CTRL and (right) GW simulations. Panels show (a),(b) SIC, (c),(d) MLD, (e),(f) surface sea–air temperature difference (sea–air ΔT), (g),(h) sensible heat flux (SHF), (i),(j) latent heat flux (LHF), and (k),(l) wind mixing energy (WME). The thin colored lines are individual ensemble members. The horizontal black line is the time mean of all CTRL ensemble members. In the CTRL panels the gray shading indicates ± 1 standard deviation from that mean. In the GW panels the thick purple line is the median of the ensemble members, the thick black line in (b) is the observed SIC from HadISST (Rayner et al. 2003), and the vertical gray blocks indicate the periods used for normal (1970–81) and reduced (2008–19) sea ice years; red dots and yellow diamonds indicate the high and low sampling years in GW, respectively.

$\text{Ice}_{\text{high_ctrl}}$ and $\text{Ice}_{\text{low_ctrl}}$. Note the sea ice concentration (SIC) in box A is significantly different between $\text{Ice}_{\text{high_ctrl}}$ and $\text{Ice}_{\text{low_ctrl}}$ using a t test (Fig. S1 in the online supplemental material).

For the GW ensemble of transient experiments, we pick two periods, 1970–81 and 2008–19 (Fig. 2b). The former is selected

to represent a “normal” sea ice state, when observed sea ice concentrations were typical of the twentieth century; the latter is selected to represent a “reduced” sea ice state, typical of the early twenty-first century, which has seen a decline in observed Arctic sea ice extent (e.g., Cavalieri and Parkinson 2012). High

and low sea ice years are then selected from these so-called normal and reduced periods by taking the mean plus and minus one standard deviation in box A. Here we take high years in the normal period for the sea ice high composite, and low years in the reduced period for the sea ice low composite, so our low sea ice years are affected by both sea ice retreat and global warming (in contrast to our low sea ice years from CTRL ensemble). Note that a comparison of years with high and low sea ice extents from both periods has also been made and its results are consistent with our primary analysis, so for clarity is not discussed further. There are 12 (14) individual years for the high (low) sea ice composites, out of 48 years for each period over the four ensemble members. We label these composites as Ice_{high_gw} and Ice_{low_gw} . Our approach is consistent across the two ensembles and allows us to isolate the effect of climate change by comparing the CTRL and GW composites.

3. Overview of changes in the wintertime atmosphere–ice–ocean environment

Figure 1 shows maps of changes in the sea ice concentration and mixed layer depth for the Ice_{low_ctrl} minus Ice_{high_ctrl} and the Ice_{low_gw} minus Ice_{high_gw} . We define the region where the SIC changes by more than 10% as the region of sea ice retreat (Figs. 1a,b). In CTRL, the largest sea ice loss lies in the western Greenland Sea and in the Iceland Sea. The mixed layer deepens in the region of sea ice retreat, with a notable anomaly in the Greenland Sea, but becomes shallower in the open ocean, farther away from the sea ice edge in the Greenland Sea Gyre (Figs. 1e,f). In GW, the loss of sea ice is enhanced almost everywhere there is ice retreat. The largest sea ice loss is also in the Greenland and Iceland Seas, but there is also a significant loss in the Barents Sea. The changes in mixed layer depth (MLD) are similar to CTRL, but with less deepening in the region of sea ice retreat and more shoaling in the Greenland Sea Gyre.

a. Sea ice and ocean surface variables

Figures 2 and 3 show the time evolution of several area-averaged variables for the areas of interest defined by box A (sea ice retreat) and box B (deep convection); see Fig. 1 for location. The simulated SICs in GW are compared with observations from HadISST (Rayner et al. 2003). The model captures the declining SIC relatively well. For box A the observations are largely within the ensemble spread as the sea ice declines (Fig. 2b), while for box B the disappearance of sea ice from the mid-1990s is well captured (Fig. 3b), although the model simulates less sea ice than observed. In general, the model is capable of reproducing climate processes in the subpolar region of interest (Shaffrey et al. 2009). The model's lower ice fraction in the region of deep convection (i.e., box B) may indicate an underestimate in the response of the model ocean to sea ice retreat.

For box A in CTRL, the variables fluctuate around a constant mean state on interannual and decadal time scales. The MLD mostly varies between 50 and 150 m with occasional years when it reaches nearly 300 m (Fig. 2c). Deeper mixed layer years are associated with great heat loss, with correlations of $r = -0.65$ with sensible heat flux (SHF; Fig. 2g), and $r = -0.68$ with latent heat flux (LHF; Fig. 2i). Deeper MLD years are accompanied by

stronger wind mixing energy (WME; Fig. 2k). Great buoyancy loss is strongly correlated with strong wind-induced mixing, as both are affected by strong winds in a low sea ice state. Another relationship is found between SIC and the temperature difference between the ocean and the overlying atmosphere ($r = 0.55$ between Figs. 2a,e), as reduced sea ice cover allows heat to escape from the ocean to the atmosphere.

Under global warming (in GW) the modeled sea ice starts to decrease slightly in the late 1970s before dropping consistently in the 2000s bringing new sea ice conditions to the Greenland Sea (Fig. 2b). MLDs greater than 150 m occur sporadically before 1990s, but are absent subsequently (Fig. 2d). This is the period when the atmosphere and ocean undergo warming, consistent with the reduction in sea ice. This leads to a decrease of 3°C in sea–air temperature difference (Fig. 2f) because the air warms more rapidly than the ocean, consistent with observations (cf. Moore et al. 2015). Consequently, there is a slight decrease in sensible heat loss over time, resulting in a decline in buoyancy loss from the ocean. Through these transient changes there are strong correlations between MLD and surface heat fluxes or wind mixing, with similar correlation coefficients to the CTRL.

Farther away from the sea ice edge in box B, the ocean is less affected by the sea ice change. The sea ice occasionally grows in this region with the concentration reaching up to 0.4 in some CTRL years (Fig. 3a) and also before 1980 in some GW years. However, in GW the concentration maximum is less than 0.1 after 1980 (except for the year 1998) and ice is totally absent after 2007 (Fig. 3b). In CTRL, the MLD has a median depth of 300 m and the extrema are deeper than 1000 m (Fig. 3c). Similar to box A, in both CTRL and GW the deeper MLD years are associated with greater surface heat loss (e.g., $r = -0.61$ between Figs. 3c and 3g, $r = -0.56$ between Figs. 3c and 3i), primarily due to the large sea–air temperature difference.

In the GW ensemble, the mixed layer gradually becomes shallower, limited to less than 400 m after 2005 (Fig. 3d). In contrast to box A, the sea–air temperature difference only reduces slightly ($<0.5^{\circ}\text{C}$) over time, indicating that warming rates in the ocean and atmosphere are similar (Fig. 3f). With the complete disappearance of the sea ice, the small change in sea–air temperature difference restricts the change in sensible heat loss (Fig. 3h). There is no evident long-term change in WME during the time. The steady state of the wind, together with only a slight decrease in sea–air temperature difference, is not sufficient to explain the large shoaling of the mixed layer (Figs. 3d and 1d). This implies a key role for the ocean circulation in modifying the intensity of convection in the Greenland Sea under climate change.

b. Ocean properties

We now examine the time evolution of ocean properties under climate change in the area of focus using GW. In box A, close to the coast of Greenland where the ocean is still partially covered by sea ice, cold and fresh surface water comes from Arctic outflows and sea ice melting, and overlies warm recirculating Atlantic Water (Fig. 4), consistent with observations (Latarius and Quadfasel 2010; Håvik et al. 2017; Renfrew et al. 2019). A stability maximum between the two layers is thus

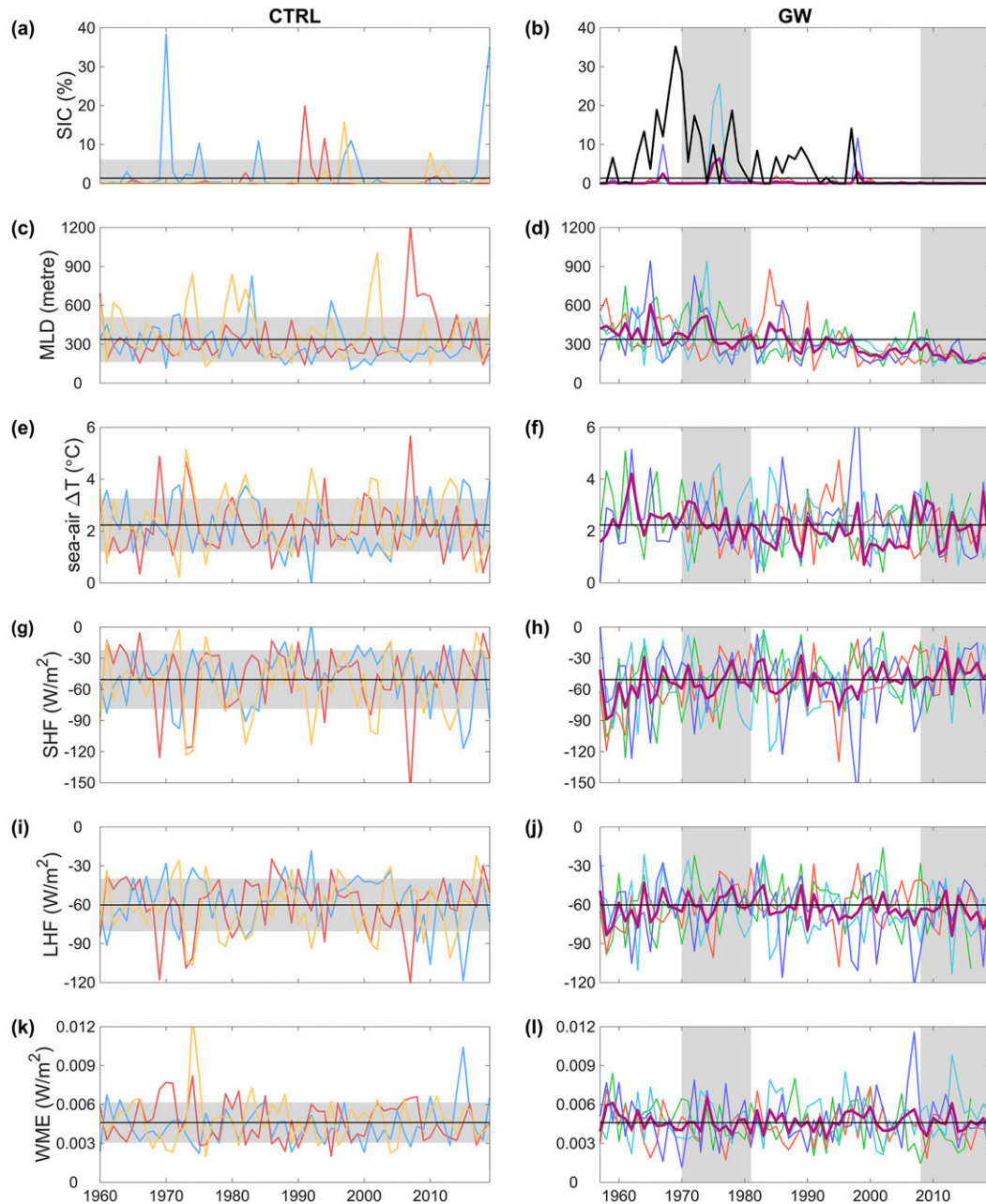


FIG. 3. As in Fig. 2, but for the time evolution of box B area-averaged variables from the (left) CTRL and (right) GW simulations.

formed at around 150 m, inhibiting vertical mixing beyond this depth (Figs. 2d and 4c). This vertical structure is stable over time, with interannual pulses of warm and saline Atlantic Water. During the 2000s there is a more continuous warming of Atlantic Water by about 0.6°C (Fig. 4a). This expansion of warmer water squeezes isotherms above and below, reducing the depth of the cold-water cap. The cold surface layer becomes warmer and fresher, increasing in temperature by 0.8°C and decreasing in salinity by 0.15 over a similar period, respectively. At these low temperatures, the decrease in salinity

dominates, which leads to a slight increase in the stability maximum (Fig. 4c), with a minor contribution from the temperature increase. Overall, this results in the ocean being more likely to restrict the depth of convective mixing further.

In box B, away from but still adjacent to the retreating sea ice region, there is evidence that ocean convection is more active: the isentropes and isopycnals are approximately vertical down to around 500-m depth (Fig. 5). The relatively warm and saline intermediate Atlantic Water is mixed with cold and fresh surface water, with some interannual variability in temperature

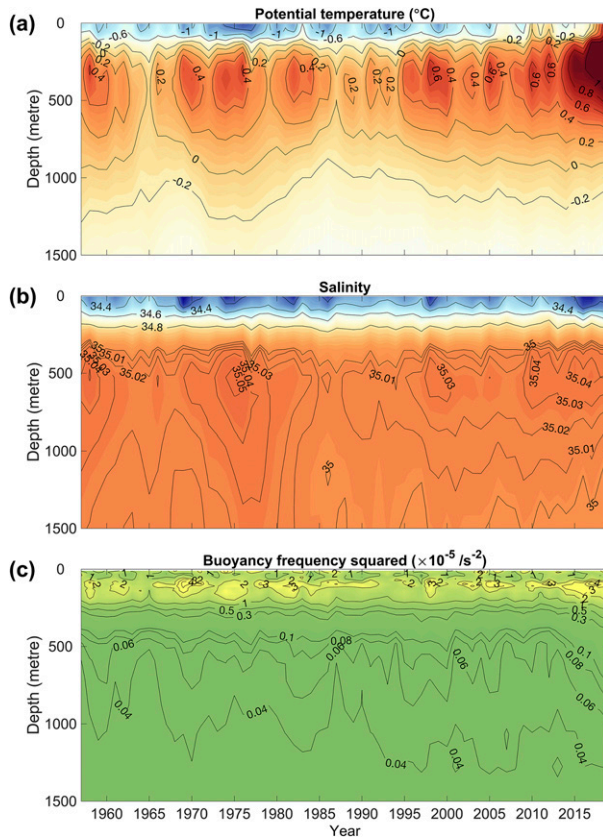


FIG. 4. Time evolution of the box A-averaged ocean (a) temperature, (b) salinity, and (c) buoyancy frequency squared for one ensemble member in GW. Colors are the contoured field, with the values as labeled.

and salinity. Note the mixed layer becomes warmer and more saline during the period especially from the 2000s. This is also when the warming is taking place in box A, but for box B the warming is more dramatic and overshadows the interannual variability in the 2010s. This upper-ocean warming enhances the stability maximum at around 500-m depth; that is, a stronger warming in the upper part of the ocean leads to a more buoyant surface layer and thus a more stratified column that inhibits or restricts the depth of convection.

4. The response of surface variables to wintertime sea ice retreat

To explore differences in atmosphere–ice–ocean properties across the zone of sea ice retreat, we select a latitudinal section at 72.5°N (cf. Fig. 1) where we find large sea ice retreat close to the region of deep convection (Marshall and Schott 1999). Figure 6 illustrates cross sections of surface variables from the CTRL ensemble (Ice_{high_ctrl} and Ice_{low_ctrl} ; left panel); and from the GW ensemble (Ice_{high_gw} and Ice_{low_gw} ; right panel). Each panel shows the SIC for the high and low sea ice composites (dashed lines), so the difference between these marks the zone of sea ice retreat.

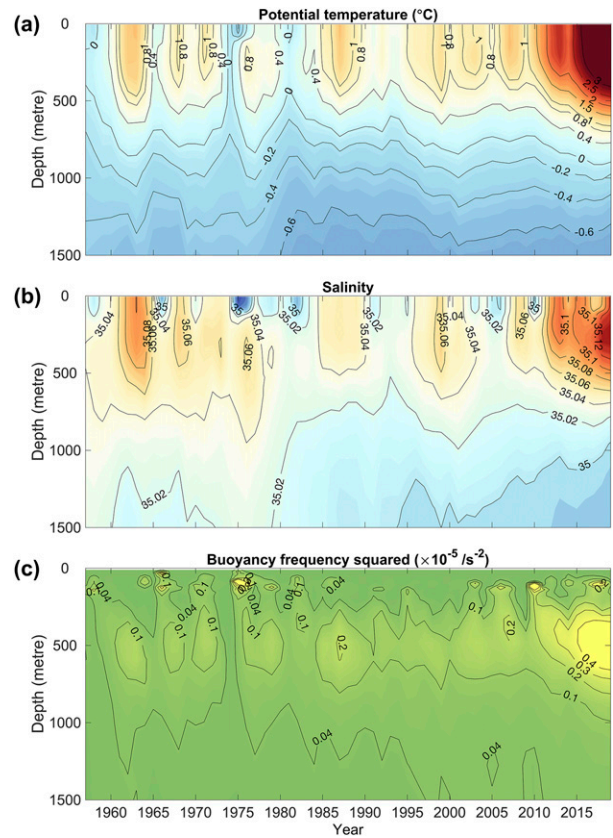


FIG. 5. As in Fig. 4, but for the time evolution of the box B-averaged values. Note that the contour intervals are different from Fig. 4.

In the high ice cases (Ice_{high_ctrl} and Ice_{high_gw}), the surface variables in both ensembles are generally qualitatively similar along this cross section. The deepest mixing happens away from, but adjacent to, the sea ice edge (Figs. 6a,b). The SHF and LHF have minima over the highest SSTs at 15°E and secondary minima at the ice edge (most prominently for GW), while WME, SST and SAT increase in magnitude from the ice-covered region to the open ocean. When it comes to the low ice cases (Ice_{low_ctrl} and Ice_{low_gw}), the sea ice edge retreats westward by about 10°, resulting in a westward retreat of the sections for surface heat fluxes, wind-induced mixing, and ocean and air surface temperatures correspondingly. This leads to important differences in the region of sea ice retreat.

There are also differences in high and low sea ice conditions between the CTRL and GW ensembles: the ice cover in CTRL is broader than that in GW, particularly in the high ice cases (Fig. 6; see also Fig. S2). This difference in ice cover is mainly attributed to the different RCP scenario forcings. For the high ice cases, mixed layer and surface variables are similar in both ensembles along the longitude range, except for at the ice edge where surface heat loss and wind mixing energy are relatively stronger in the Ice_{high_gw} case (Figs. S2g–l). This similarity in the two ensembles is also found in the low ice cases, except for an ocean surface warming resulting from the anthropogenic forcing

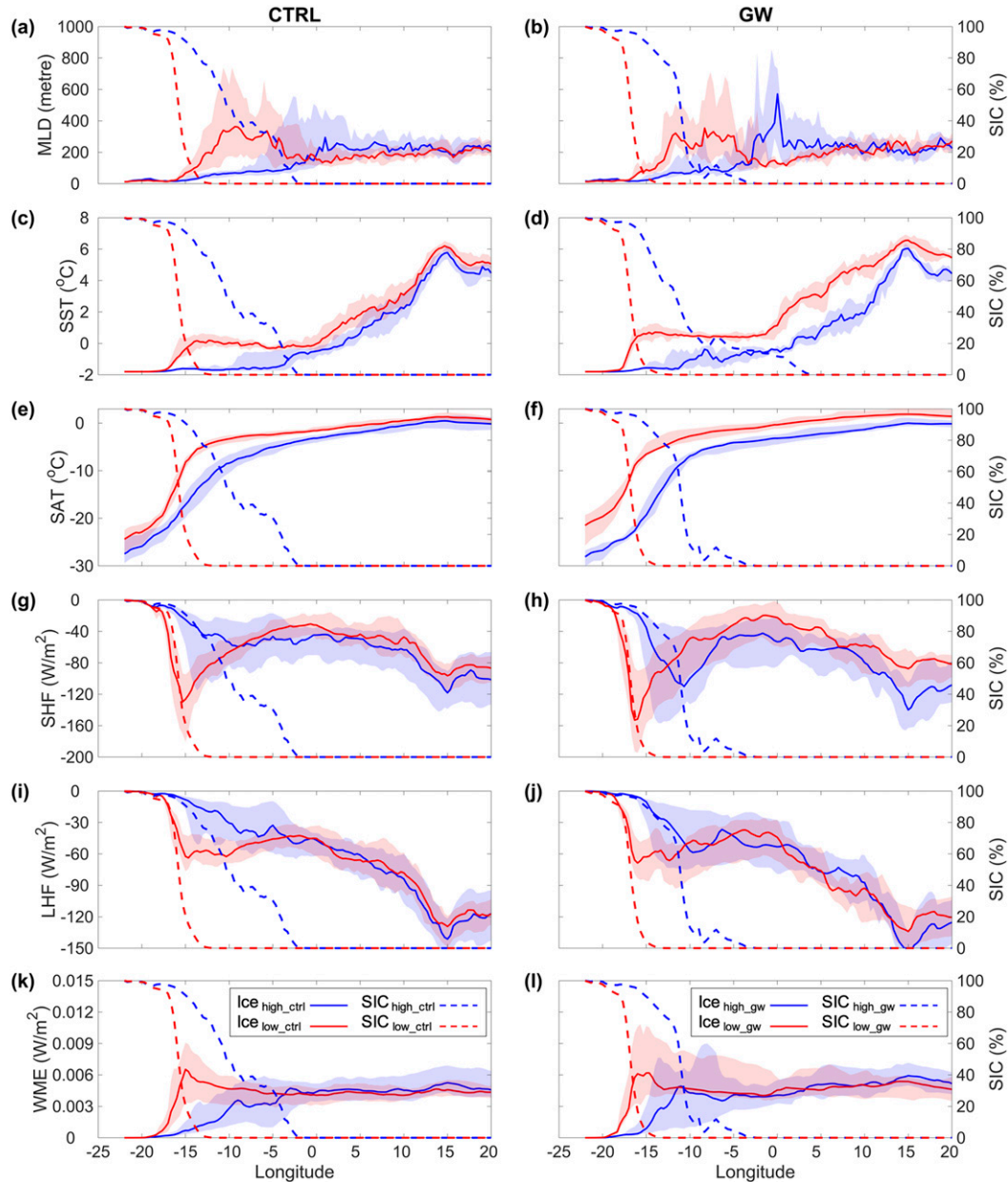


FIG. 6. Median surface variables along ocean cross sections at 72.5°N from the (left) CTRL and (right) GW simulations. Shown are (a),(b) MLD, (c),(d) SST, (e),(f) surface air temperature (SAT), (g),(h) SHF, (i),(j) LHF, and (k),(l) WME in the high (blue) and low (red) sea ice conditions (solid lines). The shading marks the 25% and 75% quantiles. Each panel also has the SIC in the high (blue dashed line) and low (red dashed line) sea ice conditions (right-hand axes); the length of the section shown is about 1470 km.

(Fig. S2d). The following subsections go into more detail first for CTRL and second for GW.

a. Surface variables during high and low sea ice states in CTRL

In the region of sea ice retreat (17°–3°W), the mixed layer in the $\text{Ice}_{\text{low_ctrl}}$ case is significantly deeper than that in the $\text{Ice}_{\text{high_ctrl}}$ case (by up to 300 m) in response to negative sea ice anomalies

(Fig. 6a). Both the surface ocean and atmosphere are warmer during the $\text{Ice}_{\text{low_ctrl}}$ case than during the $\text{Ice}_{\text{high_ctrl}}$ case, especially in the region of sea ice retreat over the Greenland Sea (Figs. 6c,e). This is consistent with regional climate simulations by Pope et al. (2020). The surface ocean and air temperatures in the region of sea ice retreat warm by up to 2° and 9°C, respectively, leading to a decrease of 7°C in sea–air temperature difference (Fig. S3a). Despite this, there is a heat

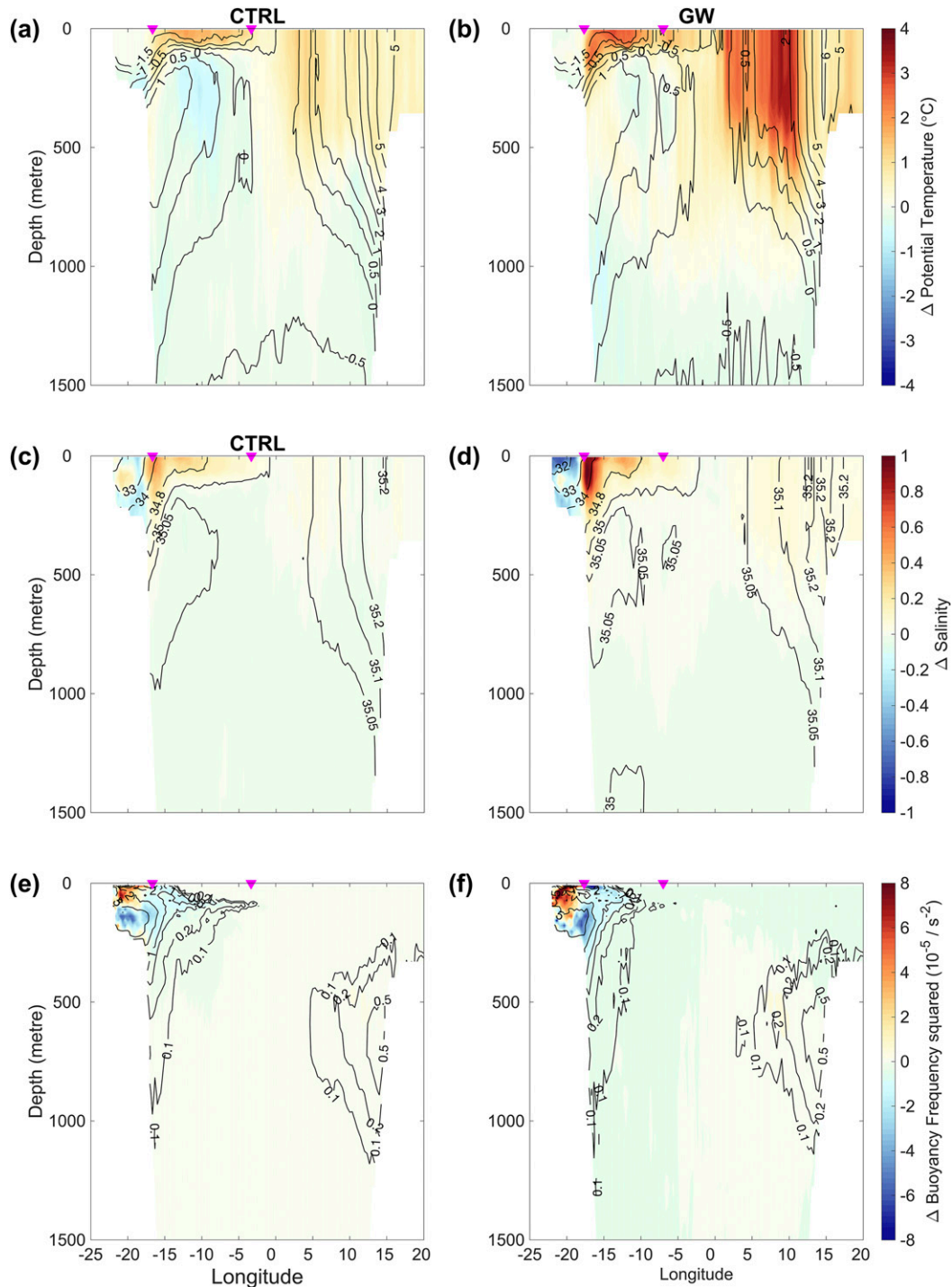


FIG. 7. Ocean cross sections at 72.5°N showing the differences between low and high sea ice conditions in the (left) CTRL and (right) GW ensembles of (a),(b) potential temperature, (c),(d) salinity, and (e),(f) buoyancy frequency squared. The black contours are the background field during high sea ice conditions. The magenta triangles at the surface indicate the region of sea ice retreat; the length of the section shown is about 1470 km.

flux minimum in this region as a consequence of the wintertime sea ice retreat (Moore et al. 2015; Pope et al. 2020). Reduced sea ice cover leads to stronger surface heat loss with the magnitude of SHF and LHF strengthened by up to 100 and 60 W m^{-2} ,

respectively (Figs. 6g,i). An enhancement in wind mixing energy also occurs (Fig. 6k) as a greater proportion of the ocean surface is directly in contact with the wind (e.g., Rainville and Woodgate 2009).

However, there is still a regionality in the response between the western (17° – 10° W) and eastern (10° – 3° W) parts of the region of sea ice retreat. The strongest enhancements of surface heat fluxes and wind mixing lie in the western part, while the deepest mixed layer is found in the mideastern part (by ~ 300 m at 10° W) where the difference in heat flux and mechanical mixing are smaller but still exist. This displacement can be attributed to a difference in the ocean stratification. A weaker stratification in the eastern part leads to greater sensitivity to atmospheric forcing (Fig. 7).

Differences in the ocean interior between the $\text{Ice}_{\text{low_ctrl}}$ and $\text{Ice}_{\text{high_ctrl}}$ cases are relatively small, the MLD shoals slightly (~ 20 m) in $\text{Ice}_{\text{low_ctrl}}$. There is also a slight decrease in SHF in the $\text{Ice}_{\text{low_ctrl}}$ case resulting from a minor increase in sea surface and surface air temperatures. These differences are located adjacent to the sea ice edge in the $\text{Ice}_{\text{high_ctrl}}$ case but are farther away in the open ocean in the $\text{Ice}_{\text{low_ctrl}}$ case. Although they are within the error range, these differences cannot be neglected as a more serious shoaling (up to 200 m; not shown) is found when moving farther north to the central Greenland Sea Gyre.

b. Surface variables during high and low sea ice states in GW

We find qualitatively similar differences in GW between the $\text{Ice}_{\text{low_gw}}$ and $\text{Ice}_{\text{high_gw}}$ composites while the region of sea ice retreat lies between 18° and 8° W. In the western part of the region (18° – 13° W), the deepening in MLD increases up to 250 m with less sea ice (Fig. 6b). This is also where the largest difference in surface heat flux and wind induced mixing occurs (Figs. 6h,j,l). The surface ocean and air temperatures increase by up to 2.5° and 12° C, respectively, resulting in a 9.5° C decrease in sea–air temperature difference that is similar to CTRL (Figs. 6d,f and Fig. S3b). Consequently, for both ensembles, the deepening of the mixed layer is primarily driven by enhancements in surface heat fluxes and wind stress impacting the ocean surface, as more ocean is exposed to the atmosphere in a reduced sea ice cover.

The situation is different in the eastern part of the region (13° – 8° W) where the ocean is partly ice-covered in the $\text{Ice}_{\text{high_gw}}$ case but totally ice-free in the $\text{Ice}_{\text{low_gw}}$ case. The biggest difference in mixing is detected in the mideastern part (by 250 m at 12° W). The surface ocean and air temperatures in the $\text{Ice}_{\text{low_gw}}$ are up to 1° and 2.5° C higher, respectively, which leads to a 1.5° C decrease in sea–air temperature difference. This explains a weakened sensible heat loss in the $\text{Ice}_{\text{low_gw}}$.

Away from the region of sea ice retreat, between 5° W and 7° E, there is considerable shoaling of the mixed layer by up to 200 m (Fig. 6b) in the $\text{Ice}_{\text{low_gw}}$ state, compared with that in the $\text{Ice}_{\text{high_gw}}$ state. This anomaly is at the southern rim of the deep convection region of the Greenland Sea Gyre (the section in Fig. 1), suggesting there may be a more significant shoaling in the center of the gyre. This is indeed the case, the shoaling is ~ 400 m in the center of the gyre (not shown). The largest SST difference also occurs in the open ocean, 2° C (Fig. 6d); meanwhile, the atmosphere has a difference of 3° C (Fig. 6f). This results in a difference of up to 1° C in the sea–air temperature difference, and thus contributes to the difference in sensible heat flux (Fig. 6h). Wind-induced mixing is similar in both states in the open ocean (Fig. 6l).

5. The response of the ocean to wintertime sea ice retreat

So far we have focused on the role of forcing at the ocean surface, but the ocean's stratification and circulation determine how it responds to this atmospheric forcing. We now examine differences in ocean properties between the low and high ice cases, for both the CTRL and GW composites, across the section at 72.5° N (Fig. 7 and Fig. S4). In the background state (illustrated as contours for the high ice cases in Fig. 7), there is a cold and fresh water mass on the western shelf. Warm and saline Atlantic Water flows northward at the eastern shelf break, circulates, and returns southward along the western shelf slope (Figs. 7a,c; Renfrew et al. 2019). Strong ventilation takes place east of the region of sea ice retreat in the Greenland Sea Gyre, as isopycnals are tilted up to the ocean surface. The ventilation reaches a depth of nearly 1500 m, implying deep convection in the Greenland Sea Gyre.

a. The ocean during high and low sea ice states in CTRL

In the $\text{Ice}_{\text{low_ctrl}}$ case, the upper ocean is generally warmer than the $\text{Ice}_{\text{high_ctrl}}$ case (Fig. 7a). The top 150 m warms by 1.2° C in the region of sea ice retreat, between 17° W and 3° E (the two magenta triangles in Fig. 7). There is a salinification of 0.02 in the upper ocean, due to brine rejection through sea ice formation actively taking place in the region of reduced sea ice (Figs. S4c,d). In the wintertime, ice formation dominates and occurs most actively at the ice edge (Papritz and Spengler 2017), implying that brine rejection will increase surface salinity at the ice edge too (Figs. S3c–f). As the ice edge retreats toward Greenland, the region of enhanced surface salinity will follow it. The increased salinity decreases the stratification of the upper ocean and creates more favorable conditions for convection during low sea ice conditions. Here the near-surface salinity provides the dominant control on the mixed layer depth due to its dominance in determining the density at these temperatures (as also found in observations; e.g., Ronski and Budéus 2005; Latarius and Quadfasel 2010, 2016). Near-surface water becomes denser with the disappearance of sea ice (not shown), which therefore promotes a deeper convection. This is particularly true near the surface where there is a minimum in stratification (e.g., in box A; see Fig. 8).

East of the region of sea ice retreat, there is a broad warming and salinification in the upper ocean (above 800 m or so) in the $\text{Ice}_{\text{low_ctrl}}$ case compared with the $\text{Ice}_{\text{high_ctrl}}$ case. Indeed, the temperature and salinity in box B are around 0.7° C and 0.01 higher in the $\text{Ice}_{\text{low_ctrl}}$ case (Figs. 9a,c). Here, density changes are more consistent with temperature changes, resulting in slightly more stable stratification from the surface to intermediate depths (Fig. 9e). In fact, the largest difference between $\text{Ice}_{\text{low_ctrl}}$ and $\text{Ice}_{\text{high_ctrl}}$ is at the stability maximum at 500 m, where $\text{Ice}_{\text{low_ctrl}}$ is less favorable for convection and appears to limit ocean mixing (cf. Figs. 6a,b).

b. The ocean during high and low sea ice states in GW

In the GW ensemble, the ocean response differences between the $\text{Ice}_{\text{low_gw}}$ and $\text{Ice}_{\text{high_gw}}$ composites are qualitatively similar to those in the CTRL ensemble, but generally intensified

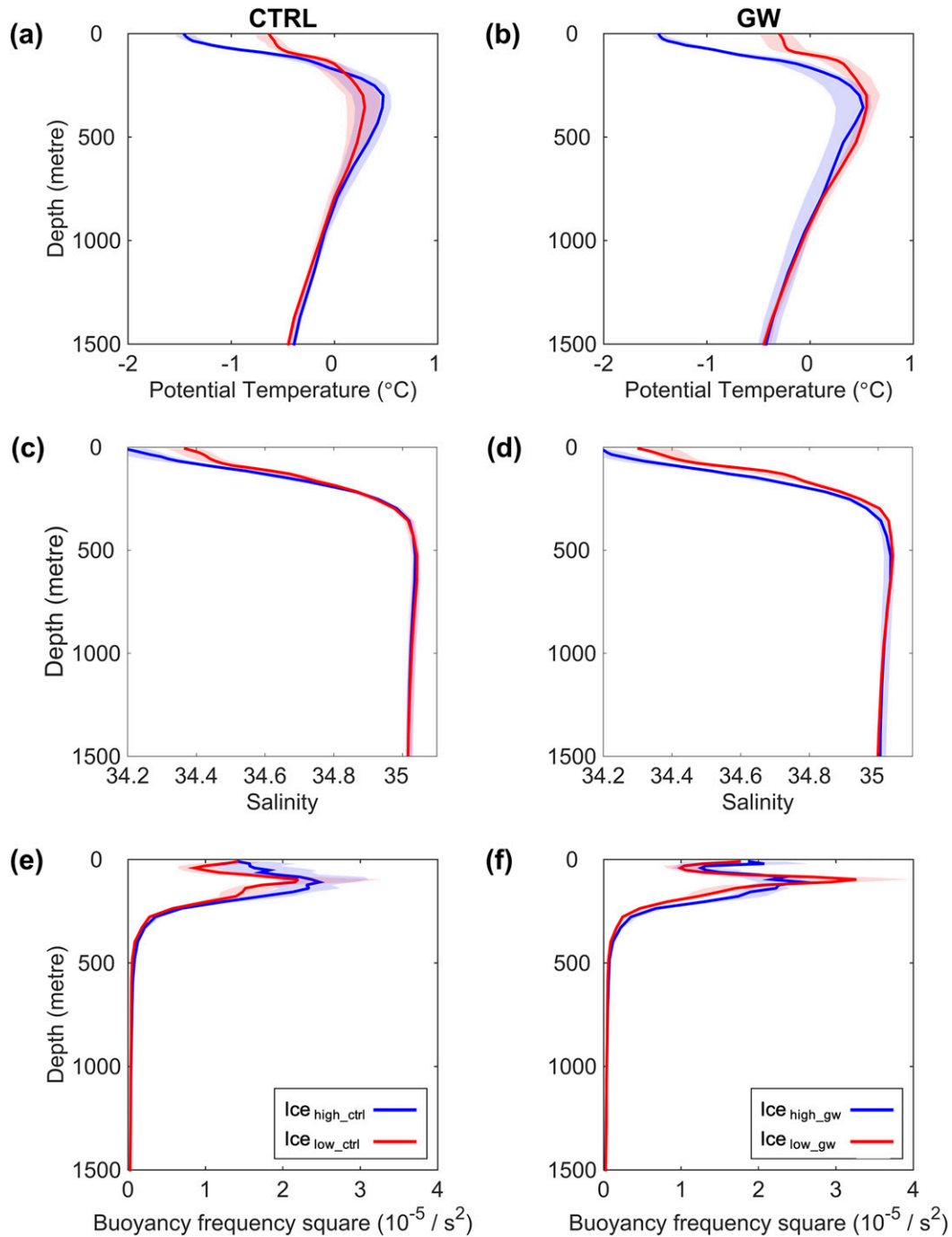


FIG. 8. Box A-averaged median profiles for the (left) CTRL and (right) GW ensembles showing (a),(b) potential temperature, (c),(d) salinity, and (e),(f) buoyancy frequency squared (N^2) in the high (blue) and low (red) sea ice conditions. The shading marks the 25% and 75% quantiles.

(e.g., Figs. 7b,d). The large amount of sea ice melting on the Greenland Sea shelf in $\text{Ice}_{\text{low_gw}}$ (23° – 20° W) leads to significant freshening, although not over the region of sea ice retreat. Another intensification is in the western part of the region of reduced sea ice, between 18° and 13° W, where a

very strong salinity increase is caused by brine rejection. This is around the ice edge in the $\text{Ice}_{\text{low_gw}}$ case (the left magenta triangle in Fig. 7b), overwhelming the warming in the same region to destabilize the upper ocean for deeper convection (Fig. 7f).

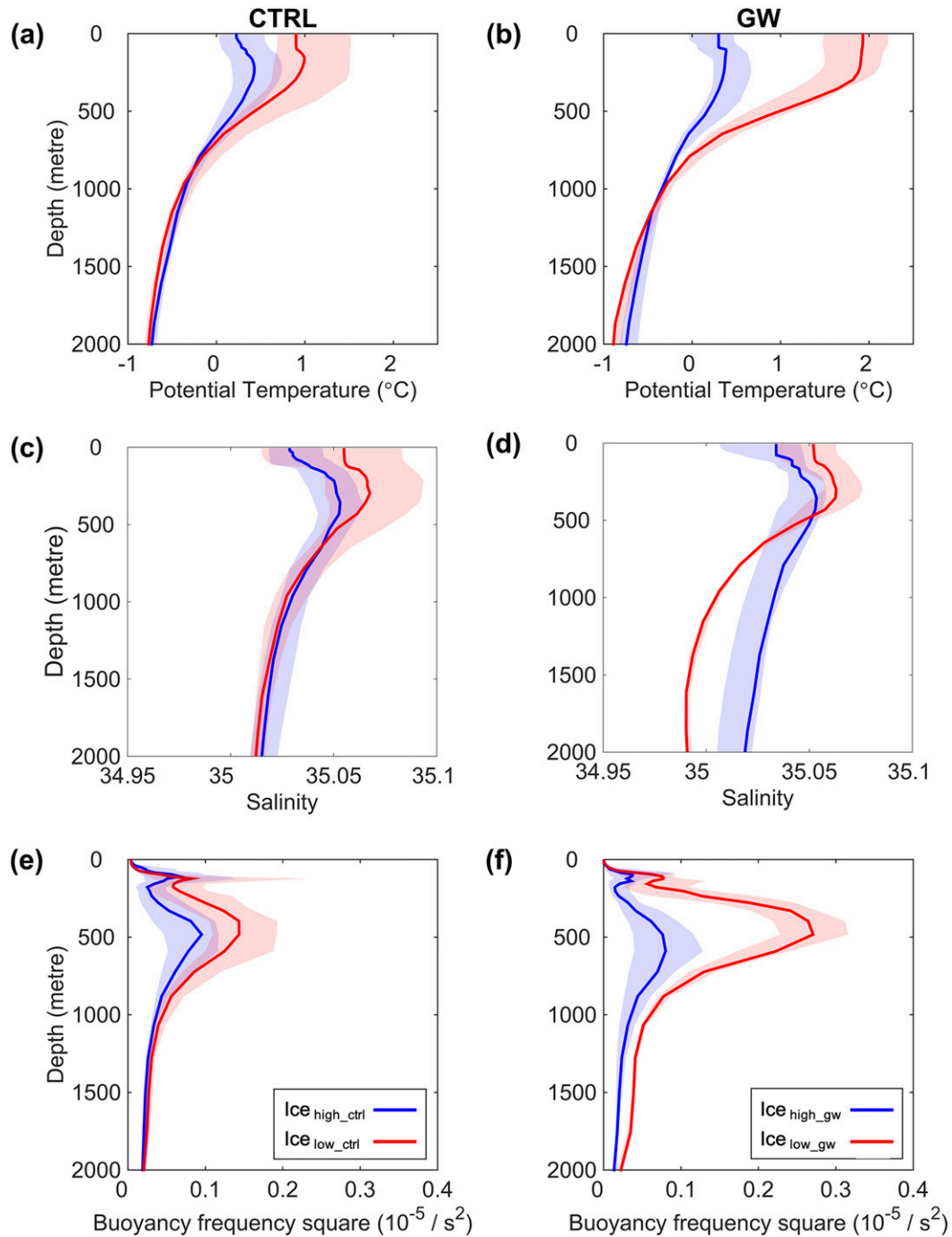


FIG. 9. Box B-averaged median profiles for the (left) CTRL and (right) GW ensembles showing (a),(b) potential temperature, (c),(d) salinity, and (e),(f) buoyancy frequency squared (N^2) in the high (blue) and low (red) sea ice conditions. The shading marks the 25% and 75% quantiles.

The most striking feature of the $\text{Ice}_{\text{low_gw}}$ and $\text{Ice}_{\text{high_gw}}$ difference is the warmer incoming Atlantic Water, between 0° and 7°E , up to 3°C higher and reaching down to 1200 m or so (Figs. 7b and 9b). This feature is consistent with observations of a warming trend in the Greenland Sea over the past three decades (Brakstad et al. 2019). The salinity of the northward

Atlantic Water is 0.05 higher in GW than in CTRL. The warmer and more saline incoming water is consistent with the warming of Atlantic inflows observed in recent decades (Hakkinen and Rhines 2009; Høydaalvik et al. 2013; Lauvset et al. 2018). As a consequence, the water column in the simulated upper open ocean is significantly more stratified—which will constrain

mixing and the depth of convection—with this amplified in $\text{Ice}_{\text{low_gw}}$ compared to $\text{Ice}_{\text{low_ctrl}}$ (Fig. 9f).

6. Discussion

Convection in the Nordic seas is significant for the vertical mixing of water masses, as well as the formation of the dense water that feeds the overflows through Denmark Strait and the Iceland–Scotland Channels. Under the background of a rapidly changing climate, potential changes in the frequency, location, and depth of ocean convection have become a focus. There is evidence from both observations and models of significant changes in convection in response to sea ice retreat both in the recent past and in the future climate (Moore et al. 2015; Våge et al. 2018; Latarius and Quadfasel 2016; Lique et al. 2015, 2018). For the first time, our study investigates changes in ocean convection in the Nordic seas using a framework in which we can isolate the impacts of sea ice retreat from those of global warming.

a. Ocean response to wintertime sea ice retreat

The most obvious response of the ocean to sea ice retreat is enhanced mixing in the region of sea ice retreat, due to elevated surface heat loss and wind stress where the ocean is now in contact with the atmosphere, especially when sudden cold weather events take place over the region (Papritz and Spengler 2017). This finding is in agreement with the observed reventilation of Atlantic Water returning southward demonstrated by Våge et al. (2018). They note this reventilation is a counterintuitive occurrence in a warming climate. However, we have shown that it is sea ice retreat that is the decisive factor here, as the ocean is modified as much in the CTRL simulations as it is in the GW simulations. The ocean stratification also affects convection in this region, with changes in salinity from brine rejection as sea ice is formed considered important in the Greenland Sea (Marshall and Schott 1999; Ronski and Budéus 2005). As the sea ice retreats, although less sea ice occupies the region, brine rejection can take place more actively, consequently creating a less stratified water column.

Interestingly, the deepest mixing does not occur at the location where the strongest atmospheric forcing occurs, demonstrating the role of ocean stratification. The most active atmosphere–ocean coupling is located in the western part of the region, but here the ocean is relatively stratified. Farther offshore where the ocean is less stratified, the ocean can be destabilized with sufficient buoyancy loss and the strongest deepening of convection takes place. Away from the sea ice edge, in the eastern part, the deepening of mixing decreases mainly due to the small difference in buoyancy and wind forcing compared between high and low sea ice states (Fig. 6). The sensitivity of ocean convection to changing atmospheric forcing in the Greenland Sea was investigated by Moore et al. (2015), who found that mixing strengthens moderately with increasing atmospheric forcing, until it exceeds a threshold, determined by background stratification, whereupon it becomes more sensitive. Our work supports the one-dimensional simulations of Moore et al. (2015), in that deeper mixing occurs in the mideast region of sea ice retreat (at 10°W in Fig. 6a and 12°W in Fig. 6b), as sufficient buoyancy loss exceeds the local

threshold. However, in the west (close to the new location of the ice edge) where the ocean is relatively stratified, or to the east where atmospheric forcing increases very little, the mixing only deepens moderately since the forcing is under the local threshold for rapid deepening.

b. Ocean response to global warming

Under anthropogenic forcing (in GW), sea ice retreats not only through interannual variability, but also as a consequence of the warming climate. The most pronounced effect is found away from the region of sea ice retreat, toward the Greenland Sea Gyre (e.g., in box B; see Fig. 9) where sea ice production is not an important driver for convection (Brakstad et al. 2019). Here the convective depth is slightly restricted as sea ice retreats, but climate warming significantly amplifies this feature. This remarkable shoaling is due to increased ocean stratification from considerable warming of the upper ocean (Figs. 7a,b and 9b), which is consistent with observations (Latarius and Quadfasel 2010; Lauvset et al. 2018; Selyuzhenok et al. 2020).

In contrast to the ocean interior, we find a generally qualitatively similar ocean response from global warming in the region of sea ice retreat (e.g., in box A; see Fig. 8). There is some evidence of the caveat of global warming: a reduction in ocean heat loss (Fig. 2h), and a persistent upper-ocean warming since the late 1990s (Fig. 4a) that has led to an increase in the subsurface ocean stratification maximum (Fig. 8f). However, these anthropogenic effects are overshadowed by the effects of the sea ice retreat, as illustrated by similar differences in the high and low ice states in CTRL and GW (e.g., see Fig. 6 or Fig. S2). This implies a limited and minor contribution of global warming in the region of sea ice retreat over recent decades.

c. Implications

There are two regions considered as the main sources of Denmark Strait Overflow water that feeds the lower limb of the Atlantic meridional overturning circulation (AMOC). One is the western boundary region, where the East Greenland Current carries transformed Atlantic-origin water to the Denmark Strait (Harden et al. 2016). The other is the interior gyres of the Iceland and Greenland Seas, where deep open-ocean convection produces Arctic Intermediate to Deep Water that contributes to Denmark Strait Overflow Water (Mastropole et al. 2017).

As sea ice continues to retreat under global warming, we may expect to see a reduction of water mass modification in the central Greenland Sea, as a result of reduced atmospheric forcing (Moore et al. 2015) and considerable upper-ocean warming. This would decrease the production of Greenland Sea Intermediate Water, which has become the main product of convection in the Greenland Sea (Karstensen et al. 2005; Jeansson et al. 2017). Sea ice retreat has also reduced the atmospheric forcing in the Iceland Sea Gyre, implying a reduction of water mass modification there too (Moore et al. 2015). In contrast, the deepening of mixing in the boundary current region, under the region of sea ice retreat, will allow recirculating Atlantic Water to be directly reventilated [as seen in Våge et al. (2018)], that is, directly increasing the density of water in the East Greenland Current.

Our simulations suggest that water mass modification has moved from the center of the gyre to the sloping boundary region. When convection occurs in the center of a gyre, the newly formed intermediate water needs to be transported to the boundary region before being exported out of the region as a deep boundary current (Hansen and Østerhus 2000; Jónsson and Valdimarsson 2004). However, if convection occurs in the boundary current region, then this can potentially affect dense water being exported out as a boundary current directly. Observations and simulations have shown a weakening in the AMOC in recent decades (e.g., Sévellec et al. 2017; Caesar et al. 2018). However, these do not factor in the changes we are seeing here. The impact of a shift in where deep water is created in the Nordic seas is unknown and is a critical open question for future study.

7. Conclusions

Wintertime sea ice retreat leads to an ocean response in the region of sea ice retreat and the adjacent deep convection region. The impact is greatest in the region of sea ice retreat, where deeper ocean convection is primarily due to the loss of sea ice, which enhances turbulent heat loss and mechanical mixing. Brine rejection from sea ice production in the newly exposed waters also contributes to a weakening of stratification that promotes deeper mixing. The effect of global warming is to inhibit deep convection, as the atmosphere warms more rapidly than the ocean which inhibits heat loss. There are also large-scale changes in ocean circulation, such as over the Greenland Sea Gyre, where the upper ocean warms significantly resulting in a more stratified water column and, as a consequence, a more severe reduction in the depth of convective mixing. In contrast, closer to the coast the effect of global warming is minor compared to the effect of sea ice retreat. It is pertinent to ask whether there is a turning point where the increasing upper-ocean stratification is strong enough to resist the buoyancy loss due to sea ice retreat. Further work is required to explore the sensitivity of subpolar convection to future more extreme climate scenarios.

Acknowledgments. YW acknowledges funding from the University of East Anglia (UEA) and the China Scholarship Council (CSC), and support from the EnvEast DTP. IAR has received funding from the NERC Grant NE/N009754/1, a component of the Iceland Greenland Seas Project. The coupled climate model was developed from the Met Office Hadley Centre Model by the U.K. NERC funded High-Resolution Modelling (HiGEM) Project. The model simulations were conducted on the high-performance computing facilities of HECToR, which was provided by the University of Edinburgh. Model analysis was carried out on the High Performance Computing Cluster supported by the Research and Specialist Computing Support service at UEA. We thank three anonymous reviewers for their constructive comments to the manuscript.

Data availability statement. Data from the HiGEM transient simulations are available via the CEDA-JASMIN platform. Data from the control runs are currently stored at the University of East

Anglia. HadISST is available from <https://www.metoffice.gov.uk/hadobs/hadisst/>.

REFERENCES

- Aagaard, K., J. H. Swift, and E. C. Carmack, 1985: Thermohaline circulation in the Arctic Mediterranean Seas. *J. Geophys. Res.*, **90**, 4833–4846, <https://doi.org/10.1029/JC090iC03p04833>.
- Bengtsson, L., V. A. Semenov, and O. M. Johannessen, 2004: The early twentieth-century warming in the Arctic—A possible mechanism. *J. Climate*, **17**, 4045–4057, [https://doi.org/10.1175/1520-0442\(2004\)017<4045:TETWIT>2.0.CO;2](https://doi.org/10.1175/1520-0442(2004)017<4045:TETWIT>2.0.CO;2).
- Blindheim, J., and S. Østerhus, 2005: The Nordic Seas, main oceanographic features. *The Nordic Seas: An Integrated Perspective, Geophys. Monogr.*, Vol. 158, Amer. Geophys. Union, 11–37.
- Brakstad, A., K. Våge, L. Håvik, and G. W. K. Moore, 2019: Water mass transformation in the Greenland Sea during the period 1986–2016. *J. Phys. Oceanogr.*, **49**, 121–140, <https://doi.org/10.1175/JPO-D-17-0273.1>.
- Budéus, G., B. Cisewski, S. Ronski, D. Dietrich, and M. Weitere, 2004: Structure and effects of a long lived vortex in the Greenland Sea. *Geophys. Res. Lett.*, **31**, L05304, <https://doi.org/10.1029/2003GL017983>.
- Caesar, L., S. Rahmstorf, A. Robinson, G. Feulner, and V. Saba, 2018: Observed fingerprint of a weakening Atlantic Ocean overturning circulation. *Nature*, **556**, 191–196, <https://doi.org/10.1038/s41586-018-0006-5>.
- Carmack, E., and K. Aagaard, 1973: On the deep water of the Greenland Sea. *Deep-Sea Res.*, **20**, 687–715, [https://doi.org/10.1016/0011-7471\(73\)90086-7](https://doi.org/10.1016/0011-7471(73)90086-7).
- Cavaliere, D. J., and C. L. Parkinson, 2012: Arctic sea ice variability and trends, 1979–2010. *Cryosphere*, **6**, 881–889, <https://doi.org/10.5194/tc-6-881-2012>.
- Chatterjee, S., R. P. Raj, L. Bertino, Ø. Skagseth, M. Ravichandran, and O. M. Johannessen, 2018: Role of Greenland Sea gyre circulation on Atlantic Water temperature variability in the Fram Strait. *Geophys. Res. Lett.*, **45**, 8399–8406, <https://doi.org/10.1029/2018GL079174>.
- Conkright, M. E., R. A. Locarnini, H. E. Garcia, T. D. O'Brien, T. P. Boyer, C. Stephens, and J. I. Antonov, 2002: World Ocean Atlas 2001: Objective analyses, data statistics, and figures: CD-ROM documentation. Tech. Rep., National Oceanographic Data Center, 17 pp.
- Day, J. J., J. L. Bamber, and P. J. Valdes, 2013: The Greenland Ice Sheet's surface mass balance in a seasonally sea ice-free Arctic. *J. Geophys. Res. Earth Surf.*, **118**, 1533–1544, <https://doi.org/10.1002/jgrf.20112>.
- de Boer, A. M., E. Gavilan Pascual-Ahuir, D. P. Stevens, L. Chafik, D. K. Hutchinson, Q. Zhang, L. C. Sime, and A. J. Willmott, 2018: Interconnectivity between volume transports through Arctic straits. *J. Geophys. Res. Oceans*, **123**, 8714–8729, <https://doi.org/10.1029/2018JC014320>.
- Fahrbach, E., J. Meincke, S. Osterhus, G. Rohardt, U. Schauer, V. Tverberg, J. Verduin, and R. A. Woodgate, 2001: Direct measurements of volume transports through Fram Strait. *Polar Res.*, **20**, 217–224, <https://doi.org/10.1111/j.1751-8369.2001.tb00059.x>.
- Hakkinen, S., and P. B. Rhines, 2009: Shifting surface currents in the northern North Atlantic Ocean. *J. Geophys. Res.*, **114**, C04005, <https://doi.org/10.1029/2008JC004883>.
- Hansen, B., and S. Østerhus, 2000: North Atlantic–Nordic seas exchanges. *Prog. Oceanogr.*, **45**, 109–208, [https://doi.org/10.1016/S0079-6611\(99\)00052-X](https://doi.org/10.1016/S0079-6611(99)00052-X).

- Harden, B. E., and Coauthors, 2016: Upstream sources of the Denmark Strait overflow: Observations from a high-resolution mooring array. *Deep-Sea Res. I*, **112**, 94–112, <https://doi.org/10.1016/j.dsr.2016.02.007>.
- Håvik, L., R. Pickart, K. Våge, D. Torres, A. Thurnherr, A. Beszczynska-Möller, W. Walczowski, and W.-J. von Appen, 2017: Evolution of the East Greenland Current from Fram Strait to Denmark Strait: Synoptic measurements from summer 2012. *J. Geophys. Res. Oceans*, **122**, 1974–1994, <https://doi.org/10.1002/2016JC012228>.
- Høydaalsvik, F., C. Mauritzen, K. A. Orvik, J. H. LaCasce, C. M. Lee, and J. Gobat, 2013: Transport estimates of the western branch of the Norwegian Atlantic Current from glider surveys. *Deep-Sea Res. I*, **79**, 86–95, <https://doi.org/10.1016/j.dsr.2013.05.005>.
- Hunke, E. C., and J. K. Dukowicz, 1997: An elastic–viscous–plastic model for sea ice dynamics. *J. Phys. Oceanogr.*, **27**, 1849–1867, [https://doi.org/10.1175/1520-0485\(1997\)027<1849:AEVPMF>2.0.CO;2](https://doi.org/10.1175/1520-0485(1997)027<1849:AEVPMF>2.0.CO;2).
- Jeansson, E., A. Olsen, and S. Jutterström, 2017: Arctic Intermediate Water in the Nordic seas, 1991–2009. *Deep-Sea Res. I*, **128**, 82–97, <https://doi.org/10.1016/j.dsr.2017.08.013>.
- Jónsson, S., 1992: Sources of fresh water in the Iceland Sea and the mechanisms governing its interannual variability. *ICES Mar. Sci. Symp.*, **195**, 62–67.
- , and J. Briem, 2003: Flow of Atlantic water west of Iceland and onto the North Icelandic shelf. *ICES Mar. Sci. Symp.*, **219**, 326–328.
- , and H. Valdimarsson, 2004: A new path for the Denmark Strait overflow water from the Iceland Sea to Denmark Strait. *Geophys. Res. Lett.*, **31**, L03305, <https://doi.org/10.1029/2003GL019214>.
- Karstensen, J., P. Schlosser, D. W. Wallace, J. L. Bullister, and J. Blindheim, 2005: Water mass transformation in the Greenland Sea during the 1990s. *J. Geophys. Res.*, **110**, C07022, <https://doi.org/10.1029/2004JC002510>.
- Latarius, K., and D. Quadfasel, 2010: Seasonal to inter-annual variability of temperature and salinity in the Greenland Sea Gyre: Heat and freshwater budgets. *Tellus*, **62A**, 497–515, <https://doi.org/10.1111/j.1600-0870.2010.00453.x>.
- , and —, 2016: Water mass transformation in the deep basins of the Nordic seas: Analyses of heat and freshwater budgets. *Deep-Sea Res. I*, **114**, 23–42, <https://doi.org/10.1016/j.dsr.2016.04.012>.
- Lauvset, S. K., A. Brakstad, K. Våge, A. Olsen, E. Jeansson, and K. A. Mork, 2018: Continued warming, salinification and oxygenation of the Greenland Sea gyre. *Tellus*, **70A** (1), 1–9, <https://doi.org/10.1080/16000870.2018.1476434>.
- Lipscomb, W. H., and E. C. Hunke, 2004: Modeling sea ice transport using incremental remapping. *Mon. Wea. Rev.*, **132**, 1341–1354, [https://doi.org/10.1175/1520-0493\(2004\)132<1341:MSITUI>2.0.CO;2](https://doi.org/10.1175/1520-0493(2004)132<1341:MSITUI>2.0.CO;2).
- Lique, C., H. L. Johnson, Y. Plancherel, and R. Flanders, 2015: Ocean change around Greenland under a warming climate. *Climate Dyn.*, **45**, 1235–1252, <https://doi.org/10.1007/s00382-014-2373-4>.
- , —, and —, 2018: Emergence of deep convection in the Arctic Ocean under a warming climate. *Climate Dyn.*, **50**, 3833–3847, <https://doi.org/10.1007/s00382-017-3849-9>.
- Macrandner, A., U. Send, H. Valdimarsson, S. Jónsson, and R. H. Käse, 2005: Interannual changes in the overflow from the Nordic seas into the Atlantic Ocean through Denmark Strait. *Geophys. Res. Lett.*, **32**, L06606, <https://doi.org/10.1029/2004GL021463>.
- Malmberg, S.-A., 1983: Hydrographic investigations in the Iceland and Greenland seas in late winter 1971—Deep Water Project. *Jökull Reykjavik*, **33**, 133–140.
- , and S. Jónsson, 1997: Timing of deep convection in the Greenland and Iceland Seas. *ICES J. Mar. Sci.*, **54**, 300–309, <https://doi.org/10.1006/jmsc.1997.0221>.
- Marshall, J., and F. Schott, 1999: Open-ocean convection: Observations, theory, and models. *Rev. Geophys.*, **37** (1), 1–64, <https://doi.org/10.1029/98RG02739>.
- Mastropole, D., R. S. Pickart, H. Valdimarsson, K. Våge, K. Jochumsen, and J. Girton, 2017: On the hydrography of Denmark Strait. *J. Geophys. Res. Oceans*, **122**, 306–321, <https://doi.org/10.1002/2016JC012007>.
- Meincke, J., S. Jónsson, and J. H. Swift, 1992: Variability of convective conditions in the Greenland Sea. *ICES Mar. Sci. Symp.*, **195**, 32–39.
- , B. Rudels, and H. J. Friedrich, 1997: The Arctic Ocean–Nordic seas thermohaline system. *ICES J. Mar. Sci.*, **54**, 283–299, <https://doi.org/10.1006/jmsc.1997.0229>.
- Moore, G. W. K., K. Våge, R. S. Pickart, and I. A. Renfrew, 2015: Decreasing intensity of open-ocean convection in the Greenland and Iceland Seas. *Nat. Climate Change*, **5**, 877–882, <https://doi.org/10.1038/nclimate2688>.
- Papritz, L., and T. Spengler, 2017: A Lagrangian climatology of wintertime cold air outbreaks in the Irminger and Nordic Seas and their role in shaping air–sea heat fluxes. *J. Climate*, **30**, 2717–2737, <https://doi.org/10.1175/JCLI-D-16-0605.1>.
- Pope, J. O., T. J. Bracegirdle, I. A. Renfrew, and A. D. Elvidge, 2020: The impact of wintertime sea-ice anomalies on high surface heat flux events in the Iceland and Greenland Seas. *Climate Dyn.*, **54**, 1937–1952, <https://doi.org/10.1007/s00382-019-05095-3>.
- Rainville, L., and R. A. Woodgate, 2009: Observations of internal wave generation in the seasonally ice-free Arctic. *Geophys. Res. Lett.*, **36**, L23604, <https://doi.org/10.1029/2009GL041291>.
- Rayner, N. A., D. E. Parker, E. B. Horton, C. K. Folland, L. V. Alexander, D. P. Rowell, E. C. Kent, and A. Kaplan, 2003: Global analyses of sea surface temperature, sea ice, and night marine air temperature since the late nineteenth century. *J. Geophys. Res.*, **108**, 4407, <https://doi.org/10.1029/2002JD002670>.
- Renfrew, I. A., and Coauthors, 2019: The Iceland Greenland Seas project. *Bull. Amer. Meteor. Soc.*, **100**, 1795–1817, <https://doi.org/10.1175/BAMS-D-18-0217.1>.
- Rhein, M., 1991: Ventilation rates of the Greenland and Norwegian Seas derived from distributions of the chloro-fluoromethanes F11 and F12. *Deep-Sea Res.*, **38**, 485–503, [https://doi.org/10.1016/0198-0149\(91\)90048-K](https://doi.org/10.1016/0198-0149(91)90048-K).
- Robson, J., I. Polo, D. L. R. Hodson, D. P. Stevens, and L. C. Shaffrey, 2018: Decadal prediction of the North Atlantic subpolar gyre in the HiGEM high-resolution climate model. *Climate Dyn.*, **50**, 921–937, <https://doi.org/10.1007/s00382-017-3649-2>.
- Ronski, S., and G. Budéus, 2005: Time series of winter convection in the Greenland Sea. *J. Geophys. Res.*, **110**, C04015, <https://doi.org/10.1029/2004JC002318>.
- Rudels, B., D. Quadfasel, H. Friedrich, and M.-N. Houssais, 2005: Greenland Sea convection in the winter of 1987–1988. *J. Geophys. Res.*, **94**, 3223–3227, <https://doi.org/10.1029/JC094iC03p03223>.
- Schlosser, P., G. Bönisch, M. Rhein, and R. Bayer, 1991: Reduction of deepwater formation in the Greenland Sea during the 1980s: Evidence from tracer data. *Science*, **251**, 1054–1056, <https://doi.org/10.1126/science.251.4997.1054>.
- Selyuzhenok, V., I. Bashmachnikov, R. Ricker, A. Vesman, and L. Bobylev, 2020: Sea ice volume variability and water temperature in the Greenland Sea. *Cryosphere*, **14**, 477–495, <https://doi.org/10.5194/tc-14-477-2020>.
- Sévellec, F., A. V. Fedorov, and W. Liu, 2017: Arctic sea-ice decline weakens the Atlantic meridional overturning circulation. *Nat. Climate Change*, **7**, 604–610, <https://doi.org/10.1038/nclimate3353>.

- Shaffrey, L. C., and Coauthors, 2009: U.K. HiGEM: The new U.K. High-Resolution Global Environment Model—Model description and basic evaluation. *J. Climate*, **22**, 1861–1896, <https://doi.org/10.1175/2008JCLI2508.1>.
- , and Coauthors, 2017: Decadal predictions with the HiGEM high resolution global coupled climate model: Description and basic evaluation. *Climate Dyn.*, **48**, 297–311, <https://doi.org/10.1007/s00382-016-3075-x>.
- Shindell, D., and G. Faluvegi, 2009: Climate response to regional radiative forcing during the twentieth century. *Nat. Geosci.*, **2**, 294–300, <https://doi.org/10.1038/ngeo473>.
- Swift, J. H., and K. Aagaard, 1981: Seasonal transitions and water mass formation in the Iceland and Greenland Seas. *Deep-Sea Res.*, **28**, 1107–1129, [https://doi.org/10.1016/0198-0149\(81\)90050-9](https://doi.org/10.1016/0198-0149(81)90050-9).
- Uppala, S. M., and Coauthors, 2005: The ERA-40 Re-Analysis. *Quart. J. Roy. Meteor. Soc.*, **131**, 2961–3012, <https://doi.org/10.1256/qj.04.176>.
- Våge, K., L. Papritz, L. Håvik, M. A. Spall, and G. W. K. Moore, 2018: Ocean convection linked to the recent ice edge retreat along east Greenland. *Nat. Commun.*, **9**, 1287, <https://doi.org/10.1038/s41467-018-03468-6>.
- Vaughan, D. G., and Coauthors, 2013: Observations: Cryosphere. *Climate Change 2013: The Physical Science Basis*, T. F. Stocker et al., Eds., Cambridge University Press, 317–382, <https://doi.org/10.1017/CBO9781107415324.012>.
- Xie, P., and P. A. Arkin, 1997: Global precipitation: A 17-year monthly analysis based on gauge observations, satellite estimates, and numerical model outputs. *Bull. Amer. Meteor. Soc.*, **78**, 2539–2558, [https://doi.org/10.1175/1520-0477\(1997\)078<2539:GPAYMA>2.0.CO;2](https://doi.org/10.1175/1520-0477(1997)078<2539:GPAYMA>2.0.CO;2).